**Author(s):** Härkönen, Ville; Karttunen, Antti J.

**Title:** Ab initio computational study on the lattice thermal conductivity of Zintl clathrates [Si19P4]Cl4 and Na4[Al4Si19]

**Year:** 2016

**Version:**

**Please cite the original version:**

Härkönen, V., & Karttunen, A. J. (2016). Ab initio computational study on the lattice thermal conductivity of Zintl clathrates [Si19P4]Cl4 and Na4[Al4Si19]. Physical Review B, 94(5), Article 054310. https://doi.org/10.1103/PhysRevB.94.054310

# *Ab initio* computational study on the lattice thermal conductivity of Zintl clathrates $[Si_{19}P_4]Cl_4$ and $Na_4[Al_4Si_{19}]$

Ville J. Härkönen*
*Department of Chemistry, University of Jyväskylä, PO Box 35, FI-40014, Finland*

Antti J. Karttunen†
*Department of Chemistry, Aalto University, FI-00076 Espoo, Finland*

(Received 26 April 2016; revised manuscript received 23 June 2016; published 17 August 2016)

The lattice thermal conductivity of silicon clathrate framework $Si_{23}$ and two Zintl clathrates, $[Si_{19}P_4]Cl_4$ and $Na_4[Al_4Si_{19}]$, is investigated by using an iterative solution of the linearized Boltzmann transport equation in conjunction with *ab initio* lattice dynamical techniques. At 300 K, the lattice thermal conductivities for $Si_{23}$, $[Si_{19}P_4]Cl_4$, and $Na_4[Al_4Si_{19}]$ were found to be 43 W/(m K), 25 W/(m K), and 2 W/(m K), respectively. In the case of $Na_4[Al_4Si_{19}]$, the order-of-magnitude reduction in the lattice thermal conductivity was found to be mostly due to relaxation times and group velocities differing from $Si_{23}$ and $[Si_{19}P_4]Cl_4$. The difference in the relaxation times and group velocities arises primarily due to the phonon spectrum at low frequencies, resulting eventually from the differences in the second-order interatomic force constants (IFCs). The obtained third-order IFCs were rather similar for all materials considered here. The present findings are similar to those obtained earlier for some skutterudites. The predicted lattice thermal conductivity of $Na_4[Al_4Si_{19}]$ is in line with the experimentally measured thermal conductivity of recently synthesized type-I Zintl clathrate $Na_8[Al_8Si_{38}]$ (polycrystalline samples).

DOI: 10.1103/PhysRevB.94.054310

## I. INTRODUCTION

The minimization of the lattice thermal conductivity is usually a desired feature when higher thermoelectric efficiency is pursued [1,2]. Zintl clathrates, also known as semiconducting clathrates, are examples of promising materials for thermoelectric applications [3–8]. Consequently, the lattice thermal conductivity of the Zintl clathrates has been studied rather intensively in the past two decades [9–30]. Several mechanisms have been proposed to explain the reduced lattice thermal conductivity values in the Zintl clathrates. In particular, lattice thermal conductivity values as low as ∼1 W/m K at 150 K have been obtained experimentally for some silicon clathrates [7,16] (single-crystal samples). Recent experimental and computational studies have given rise to different points of view for the reasons behind the reduction of the lattice thermal conductivity in various Zintl clathrates [25,27]. In Ref. [25] it was concluded that the reduction of the lattice thermal conductivity of $Ba_8Si_{46}$ is mostly due to harmonic phonon spectrum, while in Ref. [27] focusing on $Ba_8Ga_{16}Ge_{30}$, the reduction was suggested to arise mainly from rather short relaxation times (RTs). This work brings further perspectives on these issues by using computational techniques applied to two different types of Zintl clathrates.

Yet another class of crystalline solids studied as promising thermoelectric materials are the so-called skutterudites [31–36]. Recently, some skutterudites have been studied by using the same methodology as in the present work [37,38]. The results obtained here are compared with those obtained earlier for skutterudites [37,38] and it seems that in some skutterudites, the reduction of the lattice thermal conductivity appears to be due to similar reasons as in some Zintl clathrates. Thus, in addition to elucidating some of the mechanisms behind the reduced lattice thermal conductivity in some Zintl clathrates, the present work confirms in part that related mechanisms may be valid for a larger class of crystalline solids.

In this work, we study the lattice thermal conductivity of the silicon clathrate framework $Si_{23}$ (sometimes denoted as VIII or $Si_{46}$-VIII) and two hypothetical Zintl clathrate structures $[Si_{19}P_4]Cl_4$ and $Na_4[Al_4Si_{19}]$. The Zintl clathrates have been obtained by adding guest atoms and framework heteroatoms in the $Si_{23}$ structure. All the considered structures possess the same space group symmetry. This facilitates the comparative analysis of these materials because some quantities for them are identical due to symmetry reasons. Type-I Zintl clathrates $A_8[Al_8Si_{38}]$ ($A$ = Na, K, Rb, Cs) and $A_8[Ga_8Si_{38}]$ ($A$ = K, Rb, Cs) have been recently synthesized [39–41]. The thermoelectric properties of the synthesized silicon clathrates have also been investigated and they show rather low thermal conductivity (about 2 W/(m K) for $Na_8[Al_8Si_{38}]$ and below 0.5 W/(m K) for $K_8[Ga_8Si_{38}]$ at $T$ = 300 K, polycrystalline samples). The low thermal conductivity is promising considering thermoelectric applications, but further optimization of the composition (doping) is required to improve their thermoelectric properties.

We apply Boltzmann transport equation (BTE) approach implemented in the open source program package SHENGBTE. The harmonic phonon eigenvalues and eigenvectors used in the lattice thermal conductivity calculations are obtained by using density functional perturbation theory as implemented in the QUANTUM ESPRESSO (QE) program package. In particular, third-order interatomic force constants (IFCs) and quantities within the harmonic approximation are analyzed in order to understand their role in the reduction of lattice thermal conductivity. The results indicate that in the studied structures,

*ville.j.harkonen@jyu.fi
†antti.j.karttunen@iki.fi

 

the increased anharmonicity can be mostly explained by harmonic quantities. Hence, the rather low lattice thermal conductivity values do not necessarily indicate exceptionally strong third-order IFCs. In this work, a quantity is discussed as anharmonic if it is calculated by using third- or higher-order interatomic force constants (IFCs) included in the anharmonic Hamiltonian [see Eq. (3)].

## II. THEORY, COMPUTATIONAL METHODS, AND STUDIED STRUCTURES

### A. Lattice dynamics

The theory of lattice dynamics discussed in this section has been considered, for instance, in Refs. [42–44]. The notation used here is the same as in Ref. [45]. In the present approach, one assumes that the lattice Hamiltonian is of the form

$$\hat{H} = \hat{H}_0 + \hat{H}_A, \tag{1}$$

where the harmonic Hamiltonian operator $\hat{H}_0$ may be written as

$$\hat{H}_0 = \sum_{\lambda} \hbar\omega_\lambda \left(\frac{1}{2} + \hat{a}^\dagger_\lambda \hat{a}_\lambda\right), \quad \lambda \equiv \mathbf{q}j, \tag{2}$$

and the anharmonic Hamiltonian operator $\hat{H}_A$ can be written as

$$\hat{H}_A = \sum_{\lambda} V(\lambda)\hat{A}_\lambda + \sum_{n=3}\sum_{\lambda_1}\cdots\sum_{\lambda_n} \times V(\lambda_1;\ldots;\lambda_n)\hat{A}_{\lambda_1}\cdots\hat{A}_{\lambda_n}, \quad \lambda_i \equiv \mathbf{q}_i j_i. \tag{3}$$

In Eq. (3)

$$\hat{A}_\lambda = \hat{a}_\lambda + \hat{a}^\dagger_{-\lambda}, \quad -\lambda \equiv -\mathbf{q}j, \tag{4}$$

and [42]

$$V(\lambda_1;\ldots;\lambda_n) = \frac{1}{n!N^n}\left(\frac{\hbar}{2}\right)^{n/2} \frac{\Delta(\mathbf{q}_1+\cdots+\mathbf{q}_n)}{\left[\omega_{\lambda_1}\cdots\omega_{\lambda_n}\right]^{1/2}} \times \sum_{\kappa_1,\alpha_1}\sum_{l_2,\kappa_2,\alpha_2}\cdots\sum_{l_n,\kappa_n,\alpha_n} \Phi_{\alpha_1\cdots\alpha_n}(0\kappa_1;l_2\kappa_2;\ldots;l'_n\kappa'_n) \times \frac{e_{\alpha_1}(\kappa_1|\lambda_1)}{M^{1/2}_{\kappa_1}}\cdots\frac{e_{\alpha_n}(\kappa_n|\lambda_n)}{M^{1/2}_{\kappa_n}} e^{i[\mathbf{q}_2\cdot\mathbf{x}(l_2)+\cdots+\mathbf{q}_n\cdot\mathbf{x}(l_n)]}. \tag{5}$$

In Eq. (5)

$$\Phi_{\alpha_1\cdots\alpha_n}(l_1\kappa_1;\ldots;l_n\kappa_n) \equiv \left.\frac{\partial^n\Phi}{\partial x'_{\alpha_1}(l_1\kappa_1)\cdots\partial x'_{\alpha_n}(l_n\kappa_n)}\right|_{\{x'(l_i\kappa_i)=x(l_i\kappa_i)\}}, \tag{6}$$

are so-called $n$th-order atomic force constants or interatomic force constants (IFCs), which are derivatives of the potential energy $\Phi$, $\{\alpha_i\}$ are Cartesian indices, $\{\mathbf{q}_i\}$ phonon wave vectors (the wave vector times $2\pi$), $\{j_i\}$ phonon mode indices, $\{\mathbf{e}(\kappa_i|\lambda_i)\}$ phonon eigenvectors, $\{\omega_{\lambda_i}\}$ phonon eigenvalues, $\{M_{\kappa_i}\}$ atomic masses of atoms $\{\kappa_i\}$, and $\mathbf{x}(l\kappa) = \mathbf{x}(l) + \mathbf{x}(\kappa)$, where $\mathbf{x}(l)$ is the lattice translational vector and $\mathbf{x}(\kappa)$ the position vector of atom $\kappa$ within the unit cell. Furthermore, $\hat{a}^\dagger_\lambda$ and $\hat{a}_\lambda$ are so-called creation and annihilation operators for phonons, respectively.

Diagonalization of the Hamiltonian was obtained with the following expansions for displacement and momentum

$$\hat{u}_\alpha(l\kappa) = \left(\frac{\hbar}{2N^2M_\kappa}\right)^{1/2}\sum_\lambda \omega_\lambda^{-1/2} e^{i\mathbf{q}\cdot\mathbf{x}(l)} e_\alpha(\kappa|\lambda)\hat{A}_\lambda, \tag{7}$$

$$\hat{p}_\alpha(l\kappa) = -i\left(\frac{\hbar M_\kappa}{2N^2}\right)^{1/2}\sum_\lambda \omega_\lambda^{1/2} e^{i\mathbf{q}\cdot\mathbf{x}(l)} e_\alpha(\kappa|\lambda)\hat{B}_\lambda, \tag{8}$$

where $N$ is the number of $\mathbf{q}$ points in the $\mathbf{q}$ mesh and

$$\hat{B}_\lambda = \hat{a}_\lambda - \hat{a}^\dagger_{-\lambda}. \tag{9}$$

The phonon eigenvectors and eigenvalues can be obtained from the eigenvalue equation

$$\omega_j^2(\mathbf{q})e_\alpha(\kappa|\mathbf{q}j) = \sum_{\kappa',\beta} D_{\alpha\beta}(\kappa\kappa'|\mathbf{q})e_\beta(\kappa'|\mathbf{q}j), \tag{10}$$

with

$$D_{\alpha\beta}(\kappa\kappa'|\mathbf{q}) \equiv \sum_l \frac{\Phi_{\alpha\beta}(l\kappa;0\kappa')}{\sqrt{M_\kappa M_{\kappa'}}} e^{-i\mathbf{q}\cdot\mathbf{x}(l)}. \tag{11}$$

The components of the eigenvector $\mathbf{e}(\kappa|\mathbf{q}j)$ are usually chosen to satisfy the orthonormality and closure conditions [42]. A physical interpretation of the harmonic phonon eigenvectors and phase factors $e^{i\mathbf{q}\cdot\mathbf{x}(l)}$ is given in Ref. [46] and one may interpret $\mathbf{e}(\kappa|\mathbf{q}j)e^{i\mathbf{q}\cdot\mathbf{x}(l)}$ as the probability amplitude and

$$|\mathbf{e}(\kappa|\mathbf{q}j)e^{i\mathbf{q}\cdot\mathbf{x}(l)}|^2 = |\mathbf{e}(\kappa|\mathbf{q}j)|^2, \tag{12}$$

as the probability that the atom $l\kappa$ vibrates in the phonon mode $\mathbf{q}j$, which is independent of the cell index $l$.

### B. Thermal conductivity

By using the BTE approach [47,48], one may write for the lattice thermal conductivity [49–52]

$$\kappa_{\alpha\beta} = \frac{\hbar}{k_B T V}\sum_\lambda \omega_\lambda v_\alpha(\lambda)\bar{n}_\lambda(\bar{n}_\lambda+1)F_{\beta,\lambda}, \tag{13}$$

where $V$ is the volume of the unit cell, $k_B$ is the Boltzmann constant, $\mathbf{v}(\lambda)$ is the phonon group velocity, and $\bar{n}_\lambda$ the equilibrium distribution function for the state $\lambda$. The unknown term $F_{\beta,\lambda}$ is obtained by solving the iterative equation

$$F_{\alpha,\lambda} = \frac{1}{X_\lambda}\sum_{\lambda'}\sum_{\lambda''}\left[\Gamma^{\lambda''}_{\lambda\lambda'}(F_{\alpha,\lambda''}-F_{\alpha,\lambda'}) + \Gamma^{\lambda'\lambda''}_\lambda(F_{\alpha,\lambda'}+F_{\alpha,\lambda''})\right] + \frac{\hbar\omega_\lambda v_\alpha(\lambda)}{TX_\lambda}\bar{n}_\lambda(\bar{n}_\lambda+1), \tag{14}$$

where (when only three-phonon scattering is included)

$$X_\lambda \equiv \sum_{\lambda'}\sum_{\lambda''}\left(\Gamma^{\lambda''}_{\lambda\lambda'} + \Gamma^{\lambda'\lambda''}_\lambda\right). \tag{15}$$

In Eqs. (14) and (15), $\Gamma^{\lambda'\lambda''}_\lambda$ is the scattering rate for processes in which a phonon $\lambda$ vanishes and two phonons $\lambda',\lambda''$ are created. Accordingly, $\Gamma^{\lambda''}_{\lambda\lambda'}$ is the scattering rate for the opposite process. The scattering rates $\Gamma^{\lambda''}_{\lambda\lambda'}, \Gamma^{\lambda'\lambda''}_\lambda$ can be obtained, for instance,

from the golden rule or from the phonon self energy [52,53]. For example, one may write (here $\beta = 1/k_B T$)

$$\sum_{\lambda'}\sum_{\lambda''}\Gamma_{\lambda}^{\lambda'\lambda''} = 18\frac{\beta\pi}{\hbar}\sum_{\lambda'}\sum_{\lambda''}|V(\lambda;\lambda';\lambda'')|^2 \times (\bar{n}_{\lambda'}+\bar{n}_{\lambda''}+1)\delta[\omega_\lambda-\omega_{\lambda'}-\omega_{\lambda''}], \quad (16)$$

and in a similar way for the scattering rates $\Gamma_{\lambda\lambda'}^{\lambda''}$ [52,53]. In Eq. (16), the coefficients $|V(\lambda;\lambda';\lambda'')|^2$ are given by Eq. (5). By Eq. (5), the decrease of the mass of the atoms $\kappa,\kappa',\kappa''$ relative to the third-order IFCs $\Phi_{\alpha\alpha'\alpha''}(0\kappa;l'\kappa';\ldots;l''\kappa'')$ results in larger transition rates and shorter relaxation times (RTs) in general. Also, the decrease of the phonon eigenvalues $\omega_\lambda,\omega_{\lambda'},\omega_{\lambda''}$ has the same effect when other factors are fixed. These effects within the studied structures are considered in Sec. III B. The quantity $F_{\alpha,\lambda}$ is related to the RT as [51]

$$\tau_\alpha(\lambda) = \frac{T F_{\alpha,\lambda}}{\hbar\omega_\lambda v_\alpha(\lambda)}, \quad (17)$$

thus Eq. (13) can be written as

$$\kappa_{\alpha\beta} = \frac{1}{V}\sum_{\lambda} v_\alpha(\lambda)v_\beta(\lambda)c_v(\lambda)\tau_\beta(\lambda), \quad (18)$$

where the heat capacity at constant volume for the phonon state $\lambda$ may be written as

$$c_v(\lambda) = k_B\beta^2\hbar^2\omega_\lambda^2\bar{n}_\lambda(\bar{n}_\lambda+1). \quad (19)$$

The shortcomings of the method used to calculate the lattice thermal conductivity in this work are discussed in Ref. [45]. Recently, computational studies for real materials, where the temperature dependence of the IFCs is taken into account have been carried out [54,55]. This effect is neglected in the present approach and it may have some effect on the present results.

### C. Studied structures and computational details

The space group of all studied structures is $I\bar{4}3m(217)$. The silicon clathrate framework $Si_{23}$ has 23 atoms in the primitive unit cell, while the Zintl clathrates $[Si_{19}P_4]Cl_4$ and $Na_4[Al_4Si_{19}]$ have 27 atoms in the primitive unit cell. The crystallographic body-centered cubic unit cell of $[Si_{19}P_4]Cl_4$ and $Na_4[Al_4Si_{19}]$ with 54 atoms is illustrated in Fig. 1.

The parent silicon framework can be considered to be composed of fused polyhedral cages (cavities), where the vertices correspond to four-coordinated silicon atoms. The framework heteroatoms Al/P occupy the 8*c* Wyckoff position within the Si framework, while the Na/Cl guest atoms are located inside the polyhedral cages (Wyckoff position 8*c*) [6]. The $Na_4[Al_4Si_{19}]$ and $[Si_{19}P_4]Cl_4$ structures can be classified as anionic and cationic clathrates, respectively [57]. In the so-called anionic Zintl clathrates such as $Na_4[Al_4Si_{19}]$, there is a charge transfer from the less electronegative guest atoms (Na) to the framework atoms (Si-Al). In the so-called cationic Zintl clathrates such as $[Si_{19}P_4]Cl_4$, there is a charge transfer from the less electronegative framework atoms (Si-P) to the guest atoms (Cl). The bonding within the framework can be considered to be covalent, while the framework-guest interactions are of ionic nature [58].

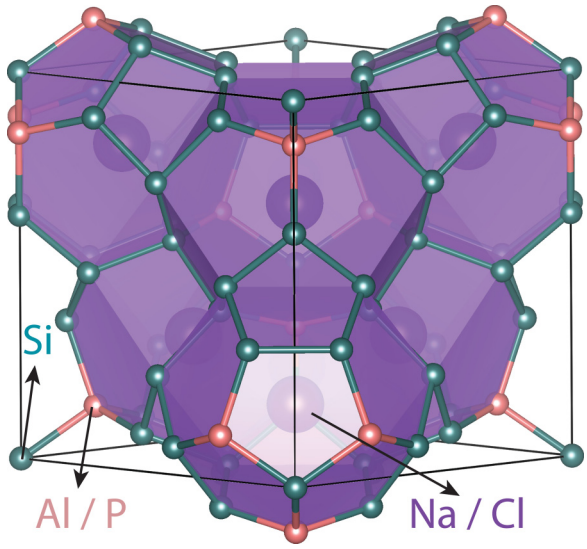


FIG. 1. The crystallographic body-centered cubic unit cell of the Zintl clathrates $[Si_{19}P_4]Cl_4$ and $Na_4[Al_4Si_{19}]$. The figure was prepared using the VESTA visualization program [56].

The *ab initio* density functional calculations to optimize the crystal structures and to calculate the phonon eigenvalues and eigenvectors were carried out with the QUANTUM ESPRESSO program package (QE, version 5.0.3) [59]. Atoms were described using ultrasoft pseudopotentials and plane-wave basis set [60]. The generalized gradient approximation (GGA) was applied by using the PBE exchange-correlation energy functionals [61]. If not otherwise mentioned, the applied computational parameters and methods were similar to those used in Ref. [45]. The results for the clathrate framework $Si_{23}$, used here for comparative analysis of the Zintl clathrates, were taken from Ref. [45]. A (6,6,6) mesh was used for the electronic **k** sampling, while (4,4,4) and (10,10,10) **q** meshes were used for phonon and lattice thermal conductivity calculations, respectively. The chosen **q** mesh (10,10,10) is a compromise between accuracy and computational requirements. For instance, for the clathrate framework $Si_{23}$ at 300 K, increasing the **q** mesh from (8,8,8) to (10,10,10) changes the lattice thermal conductivity by about 7.5%, whereas further increase from (10,10,10) to (11,11,11) changes the lattice thermal conductivity by about 1.4%. Both the lattice constants and the atomic positions of the studied structures were optimized by forcing the space group $I\bar{4}3m$. The optimized lattice constants were 10.10 Å, 10.00 Å, and 10.37 Å for $Si_{23}$, $[Si_{19}P_4]Cl_4$, and $Na_4[Al_4Si_{19}]$, respectively. The nonanalytic corrections to dynamical matrices in the limit $\mathbf{q} \to 0$ were taken into account in the QE and SHENGBTE calculations. The version 1.0.2 of SHENGBTE was used (the weighted phase space was calculated using version 1.1.0). In the lattice thermal conductivity calculations, three-phonon and isotopic scattering were included. In order to calculate the $\delta$ functions appearing, for example, in Eq. (16), some approximate representation is needed. In SHENGBTE, a Gaussian function is used to approximate the Dirac $\delta$ function and a constant called scalebroad is a proportional coefficient for the variance [52,62]. The constant scalebroad was set to 0.5 in all SHENGBTE calculations. For all structures, the third-order IFCs were calculated up to sixth-nearest neighbors

using the program THIRDORDER.PY included in the SHENGBTE distribution [63]. A (3,3,3) supercell was used to calculate the third-order IFCs with THIRDORDER.PY in all cases.

The validity of the present computational approach was assessed in Ref. [45], for instance, by comparing the calculated lattice thermal conductivity values to the experimental ones in the case of the silicon diamond structure (*d*-Si). The difference between the calculated and experimental values was about 4–13 % within the temperature range 125–300 K (higher temperatures showed the smallest differences).

## III. RESULTS AND DISCUSSION

### A. Phonon spectrum

The calculated phonon eigenvalues (dispersion relations) along high symmetry paths for the structures $Si_{23}$, $[Si_{19}P_4]Cl_4$ and $Na_4[Al_4Si_{19}]$ are shown in Fig. 2. The phonon dispersions are rather similar for all structures within the frequency range 200–500 $cm^{-1}$. For frequencies below 100 $cm^{-1}$, $Si_{23}$, and $[Si_{19}P_4]Cl_4$ show rather similar spectrum while the spectrum for $Na_4[Al_4Si_{19}]$ appears to be different. The differences

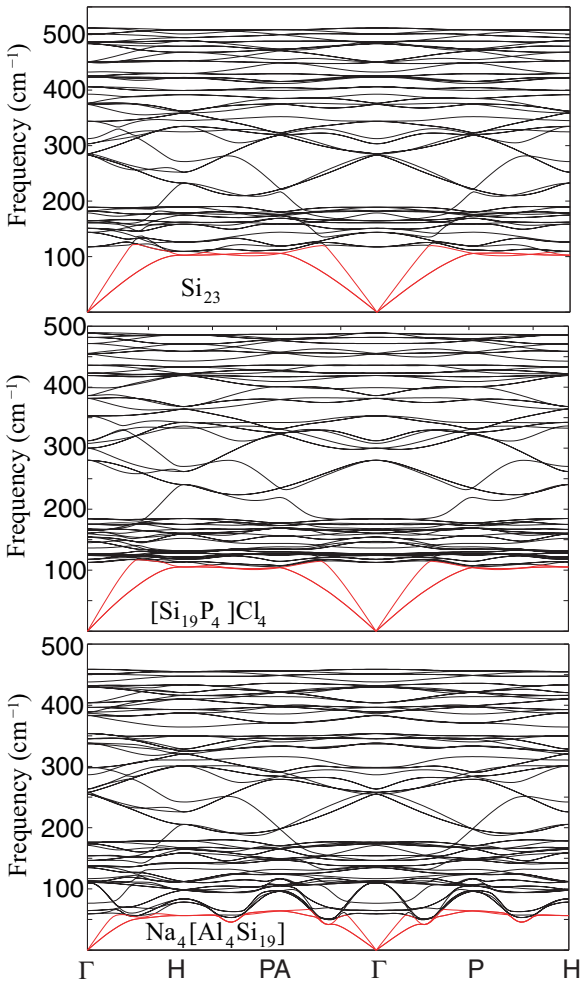


FIG. 2. Phonon eigenvalues as a function of wave vector (dispersion relations) along high symmetry paths in the first Brillouin zone for $Si_{23}$, $[Si_{19}P_4]Cl_4$, and $Na_4[Al_4Si_{19}]$. The dispersion relations for the acoustic modes are drawn in red.

between $Si_{23}$ and $[Si_{19}P_4]Cl_4$ are mostly due to the Cl guest atoms within the frequency range 100–200 $cm^{-1}$ (this can be seen from the atom projected phonon density of states considered later in this section). The maximum frequencies of acoustic modes for $Na_4[Al_4Si_{19}]$ are about half that of the corresponding values in the case of $Si_{23}$ and $[Si_{19}P_4]Cl_4$. Furthermore, the acoustic and lowest-energy optical modes of the structure $Na_4[Al_4Si_{19}]$ show oscillatory behavior, for example, along the high symmetry paths $\Gamma$–$P$ and $\Gamma$–$PA$, while in the case of $Si_{23}$ and $[Si_{19}P_4]Cl_4$ this behavior seems to be absent.

According to Eq. (10) and since both structures with guest atoms have the same exponential factors, $e^{-i\mathbf{q}\cdot\mathbf{x}(l)}$, difference of the dynamical matrix elements $\{D_{\alpha\beta}(\kappa\kappa'|\mathbf{q})\}$ is due to the second-order IFCs divided by the atomic masses $D_{\alpha\beta}(l\kappa;0\kappa') = \Phi_{\alpha\beta}(l\kappa;0\kappa')/\sqrt{M_\kappa M_{\kappa'}}$ [Eq. (11)]. After one fixes the dynamical matrix, the eigenvectors can be calculated numerically: with this and the preceding in mind one may infer that the differences in the dispersion relations for frequencies below 100 $cm^{-1}$ indicate differences in $\{D_{\alpha\beta}(l\kappa;0\kappa')\}$ between the considered structures.

In Fig. 3, the so-called atom projected density of states $\rho_\kappa(\omega) = 1/N \sum_\lambda |\mathbf{e}(\kappa|\lambda)|^2 \delta(\omega - \omega_\lambda)$ and the participation ratio (PR) defined as [25,27,64,65]

$$\mathrm{PR} = \frac{\left[\sum_\kappa |\mathbf{e}(\kappa|\lambda)|^2 M_\kappa^{-1}\right]^2}{N_a \sum_\kappa |\mathbf{e}(\kappa|\lambda)|^4 M_\kappa^{-2}} \tag{20}$$

are shown to further analyze the differences in the phonon spectrum of the studied structures.

$N_a$ is the number of atoms within the unit cell. If one considers $|\mathbf{e}(\kappa|\lambda)|^2$ as the probability distribution (Sec. II A), then $\rho_\kappa(\omega)$ may be considered as the expected value of the phonon density of states (PDOS) for each $\kappa$. It can be seen from Fig. 3 that the contribution of the framework heteroatoms (Al and P) to $\rho_\kappa(\omega)$ is rather similar to that of the Si framework atoms, when comparing all three structures. However, some differences can be identified, for instance, at the frequencies 3–6 THz. The guest atoms Cl and Na mainly contribute to the phonon modes at the frequencies below 5 THz. Further, for $Na_4[Al_4Si_{19}]$, there is a relatively large contribution of Na guest atoms at 2 THz, while an analogous contribution from the Cl guest atoms is absent in the case of $[Si_{19}P_4]Cl_4$.

The PR can be used to study the localization of the phonon modes [64]. The modes with rather local characteristics are expected to have PR values near $N_a^{-1}$ (only few atoms are displaced in the mode), while PR values of about 1 indicate the opposite. In $Si_{23}$ and $[Si_{19}P_4]Cl_4$, the PR values for the acoustic modes are approximately between 1 and 0.5, while for $Na_4[Al_4Si_{19}]$ PR values as low as 0.1 are obtained and most of the PR values for the acoustic modes are clustered between 0.1 and 0.2. This indicates that the acoustic modes of $Na_4[Al_4Si_{19}]$ seem to have more local characteristics than the acoustic modes in the other two structures.

To estimate the difference in the harmonic interactions (the wave vector dependence is the same in all cases), the dynamical matrix at $\mathbf{q} = 0$ is considered

$$D_{\alpha\alpha'}(\kappa\kappa'|0) \equiv D(\varsigma\varsigma'|0), \quad \varsigma \equiv \alpha\kappa, \quad \varsigma' \equiv \alpha'\kappa'. \tag{21}$$

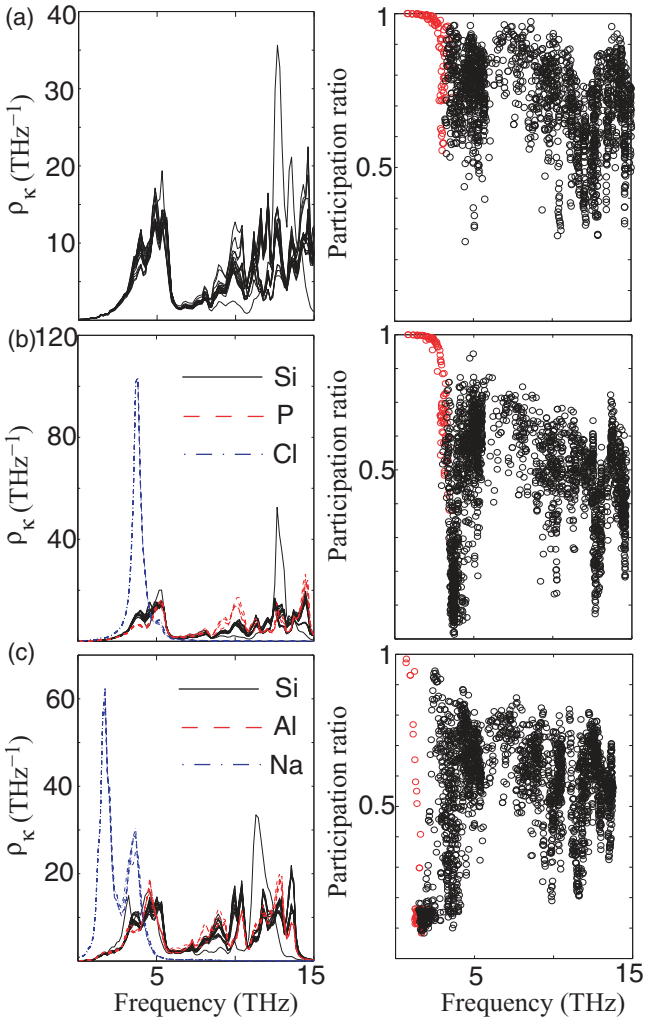


FIG. 3. Atom projected density of states $\rho_\kappa(\omega)$ and participation ratio for each structure. (a) $Si_{23}$, (b) $[Si_{19}P_4]Cl_4$, and (c) $Na_4[Al_4Si_{19}]$. The participation ratio values for the acoustic modes are drawn in red.

The phonon eigenvalues can be estimated by using the method of Gerschgorin circles [66] applied on $D(\varsigma\varsigma'|0)$. The Gerschgorin theorem states that the eigenvalues $\omega$ of $D(\varsigma\varsigma'|0)$ are contained in the following union

$$r_{\varsigma_1} \cup r_{\varsigma_2} \cup \cdots \cup r_{\varsigma_{3n}}, \tag{22}$$

with

$$|\omega^2 - D(\varsigma\varsigma|0)| \leqslant r_\varsigma, \quad r_\varsigma = \sum_{\varsigma'=1,\varsigma\neq\varsigma'}^{3n} D(\varsigma\varsigma'|0). \tag{23}$$

Here, only the Zintl clathrates are considered. All the diagonal elements $D(\varsigma\varsigma|0)$ in the case of the structure $[Si_{19}P_4]Cl_4$ are larger than those for $Na_4[Al_4Si_{19}]$. The ratio of the diagonal elements is within the interval [1.21,1.49]. Moreover, the length of the intervals, $\{r_\varsigma\}$, are larger for the clathrate $[Si_{19}P_4]Cl_4$ and the ratio is within the interval [1.16,2.50], the largest values being obtained for the guest atoms Na/Cl. Both of these observations probably favor the smaller phonon eigenvalues to be obtained for the clathrate $Na_4[Al_4Si_{19}]$. In particular, the lengths $r_{\varsigma_g}$ centered at $D(\varsigma_g\varsigma_g|0)$ have such values that there is no overlap between the diagonal elements $D(\varsigma_f\varsigma_f|0)$ and the intervals $r_{\varsigma_g}$. In the preceding, the subscripts $g$ and $f$ refer to the guest (Na/Cl) and framework atoms (P/Al/Si), respectively. The overlap of these intervals is still obtained since the lengths $r_{\varsigma_f}$ centered at $D(\varsigma_f\varsigma_f|0)$ overlap with the diagonal elements $D(\varsigma_g\varsigma_g|0)$. Thus, the bounds imposed by the Gerschgorin theorem on these dynamical matrices are not strict enough to the conclusion that there are certainly phonon eigenvalues at these lower frequencies. One may say, however, that in order to minimize the energy of the lowest phonon states it is probably favorable to minimize the diagonal elements $D(\varsigma\varsigma|\mathbf{q})$ and maybe the length of the intervals $r_\varsigma$ as well.

To summarize, the framework heteroatoms and the Si framework atoms seem to have rather similar effect on the phonon spectrum in all the studied structures. Furthermore, the Na and Cl guest atoms appear to have a rather large effect on the phonon spectrum at the frequencies below 5 THz. The Na guest atoms seem to flatten the acoustic phonon dispersion relations in a more distinct manner in comparison to the Cl guest atoms.

### B. Results for lattice thermal conductivity and related quantities

The calculated thermal conductivity values as a function of temperature for all studied structures are shown in Fig. 4. The lattice thermal conductivities for $Si_{23}$ and $[Si_{19}P_4]Cl_4$ within the temperature range 100–300 K are 282–43 W/(m K) and 122–25 W/(m K), respectively. Within the same temperature range, the lattice thermal conductivities for $Na_4[Al_4Si_{19}]$ are approximately 6–2 W/(m K). Thus, the present results indicate that the lattice thermal conductivity of $Na_4[Al_4Si_{19}]$ is reduced by a factor of about 20 in comparison to $Si_{23}$ and by a factor of about 10 in comparison to $[Si_{19}P_4]Cl_4$. The predicted lattice thermal conductivity of $Na_4[Al_4Si_{19}]$ is in line with the experimentally measured thermal conductivity of recently synthesized type-I Zintl clathrate $Na_8[Al_8Si_{38}]$ [40]. The experimental thermal conductivity of $Na_8[Al_8Si_{38}]$ was measured to be about 2 W/(m K) at 300 K (laser flash method, hot pressed pellet of polycrystalline sample). For

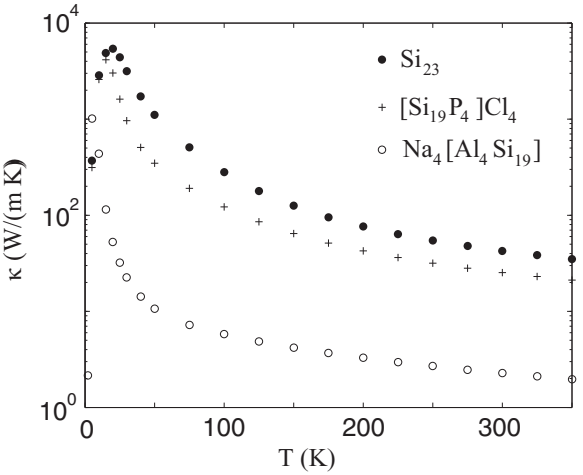


FIG. 4. Calculated lattice thermal conductivity values for the structures $Si_{23}$, $[Si_{19}P_4]Cl_4$, and $Na_4[Al_4Si_{19}]$.

a better comparison, the experimental values for the lattice thermal conductivity of single-crystal samples are needed. The electronic contribution to the thermal conductivity was estimated to be significantly less than 1% of the total thermal conductivity at all temperatures.

In Refs. [29,30], the lattice thermal conductivities obtained for $Si_{23}$ (or $Si_{46}$-VIII) were smaller by a factor of about three at 300 K in comparison to the present work (the results were obtained by using more approximate models for the lattice conductivity in comparison to the linearized BTE used here). Furthermore, the lattice thermal conductivity obtained for $Ba_8Al_{16}Si_{30}$ and $Ba_8Cu_6Si_{40}$ clathrates at 300 K in Ref. [30] were smaller by a factor of about four in comparison to $Na_4[Al_4Si_{19}]$ studied here. As discussed in Ref. [45], the lattice thermal conductivity values at relatively low temperatures have a rather poor convergence. However, the values obtained at low temperatures are included in Fig. 4 to show that the present method provides the expected form for the lattice thermal conductivity for single crystals as a function of temperature.

The lattice thermal conductivity values for each state $\lambda$ in conjunction with the RTs $\tau(\lambda)$, phonon phase space $P_3(\lambda)$ [52,67], and quantities $\xi(\lambda)$ are shown in Fig. 5. It should be noted that $\kappa(\lambda) = \xi(\lambda)\tau(\lambda)$.

For $Na_4[Al_4Si_{19}]$, the largest lattice thermal conductivity contributions of acoustic modes are rather systematically smaller in comparison to $Si_{23}$ or $[Si_{19}P_4]Cl_4$. A similar difference can be seen between the structures $Si_{23}$ and $[Si_{19}P_4]Cl_4$. $Si_{23}$ and $[Si_{19}P_4]Cl_4$ show rather similar values for

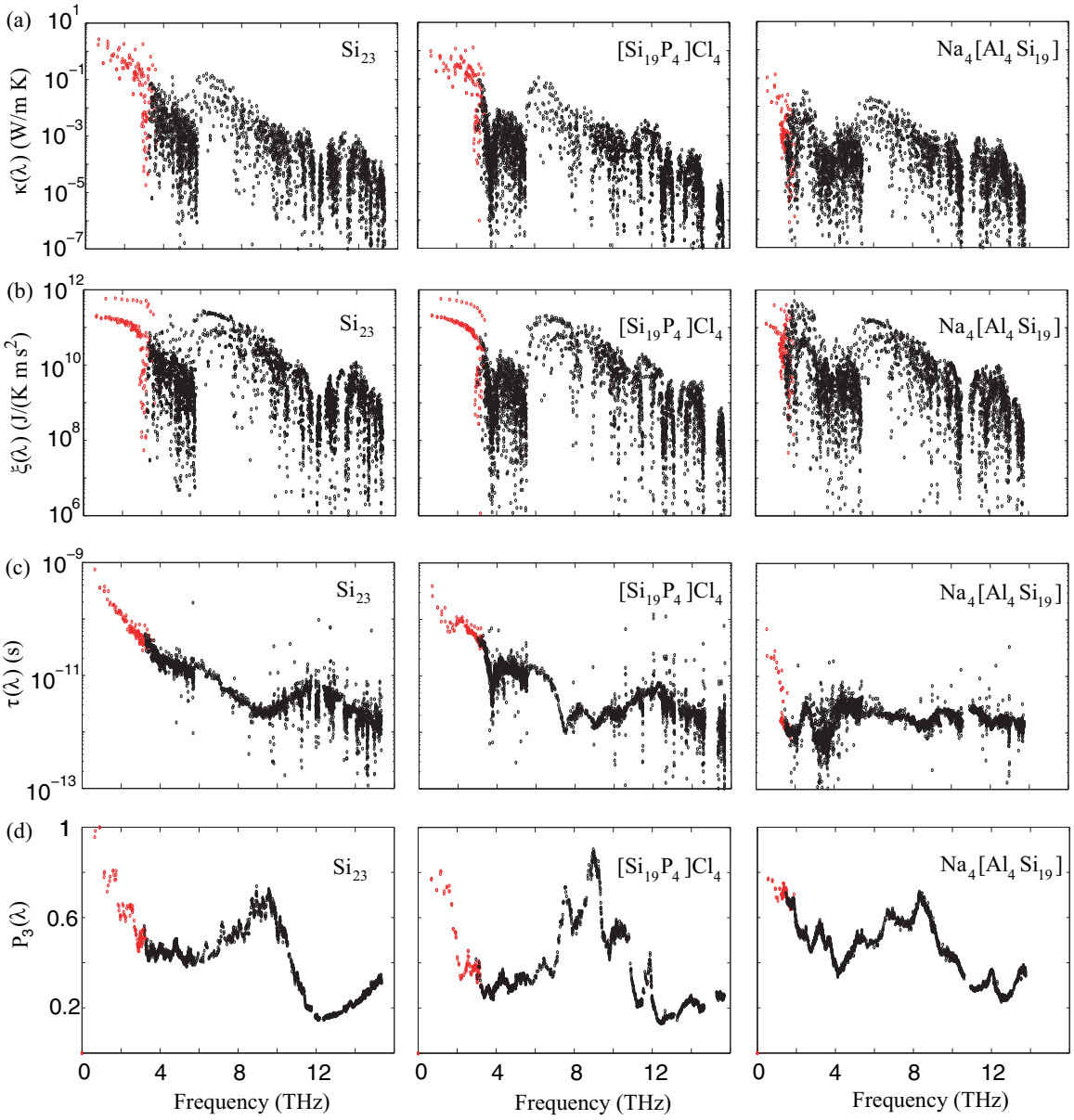


FIG. 5. Calculated values for each state $\lambda$ as a function of phonon frequency for the structures $Si_{23}$, $[Si_{19}P_4]Cl_4$ and $Na_4[Al_4Si_{19}]$ at 300 K. (a) Lattice thermal conductivity $\kappa(\lambda) = \kappa_{\alpha\alpha}(\lambda) = 1/3 \sum_\alpha \kappa_{\alpha\alpha}(\lambda)$ (negative values are not shown), (b) quantities $\xi(\lambda) \equiv 1/(3V) \sum_\alpha v_\alpha^2(\lambda) c_v(\lambda)$, (c) relaxation times $\tau(\lambda) \equiv \sum_\alpha \tau_\alpha(\lambda)$ (negative values are not shown), and (d) phonon phase space $P_3(\lambda)$. For all quantities, the acoustic modes are drawn in red and the optical modes in black. The reported $P_3(\lambda)$ values are unitless relative values obtained from $P_3(\lambda)/\max\{P_3(\lambda)|_{Si_{23}}\}$.

the quantity $\xi(\lambda)$. As in the case of lattice thermal conductivity, $Na_4[Al_4Si_{19}]$ also has a rather different distribution of values of the quantity $\xi(\lambda)$, the values for acoustic modes being mostly smaller in comparison to $Si_{23}$ or $[Si_{19}P_4]Cl_4$. This is not that surprising because the harmonic phonon spectrum for the acoustic modes of $Na_4[Al_4Si_{19}]$ is rather different in comparison to the other two structures (Fig. 2). The flattening of the acoustic modes as a function of $\mathbf{q}$ means that $\omega(\lambda)$ have smaller values for acoustic modes. This has, for example, the following effects on $\xi(\lambda)$ at fixed temperature $T_0$: smaller values of $\omega(\lambda)$ increase $\bar{n}_\lambda$ and thus $c_v(\lambda)$. The flattening decreases the group velocity $\mathbf{v}(\lambda)$, thus the flattening has opposite effect on $\mathbf{v}(\lambda)$ and $c_v(\lambda)$. In the case of $Na_4[Al_4Si_{19}]$, the change in the harmonic phonon spectrum seems to favor the reduced group velocities more than the increase of $c_v(\lambda)$, resulting in the smaller values of $\xi(\lambda)$ for acoustic modes.

The RTs, shown in Fig. 5, reveal some differences between $Si_{23}$ and $[Si_{19}P_4]Cl_4$. $Si_{23}$ has larger maximum values of $\tau(\lambda)$, in particular for acoustic modes. This seems to be the main reason for the different values of lattice thermal conductivity obtained for $[Si_{19}P_4]Cl_4$ and $Si_{23}$. The RTs for $Na_4[Al_4Si_{19}]$ are in general smaller than those obtained for $[Si_{19}P_4]Cl_4$ and $Si_{23}$. Compared with $[Si_{19}P_4]Cl_4$, the maximum values for the acoustic modes of $Na_4[Al_4Si_{19}]$ are smaller by a factor of about 10. For $[Si_{19}P_4]Cl_4$ and $Na_4[Al_4Si_{19}]$, it appears that the third-order coefficients $V(\lambda;\lambda';\lambda'')$ may have larger values than in the case of $Si_{23}$.

The distribution of phonon phase space values $P_3(\lambda) \propto \tau^{-1}(\lambda)$, also shown in Fig. 5, are rather different for all structures despite the rather similar phonon spectra for the structures $Si_{23}$ and $[Si_{19}P_4]Cl_4$. The maximum values are, perhaps surprisingly, largest for $Si_{23}$. For example, $Si_{23}$ has larger $P_3(\lambda)$ values for acoustic modes than $d$-Si [45], which probably is one of the reasons behind the smaller lattice thermal conductivity of $Si_{23}$ in comparison to $d$-Si. The maximum values of $P_3(\lambda)$ are rather similar for $[Si_{19}P_4]Cl_4$ and $Na_4[Al_4Si_{19}]$. However, for $Na_4[Al_4Si_{19}]$, the $P_3$ values for acoustic modes are more clustered than for the other structures and there are practically no values below 0.6, while for other structures there are rather many states with values smaller than this. Thus, it seems that the $P_3$ values, which are in part differing due to flattening of the acoustic modes, are one of the reasons behind the smaller RTs obtained for $Na_4[Al_4Si_{19}]$.

In Fig. 6, the third-order IFCs as a function of distance are shown. The following quantities are used in Fig. 6

$$d(0\kappa_1;l_2\kappa_2;l_3\kappa_3) \equiv |x(\kappa_1)-x(l_2\kappa_2)|+|x(\kappa_1)-x(l_3\kappa_3)|, \quad (24)$$

$$\Phi_3 \equiv \frac{1}{27}\sum_{\alpha_1,\alpha_2,\alpha_3}\left|\Phi_{\alpha_1\alpha_2\alpha_3}(0\kappa_1;l_2\kappa_2;l_3\kappa_3)\right|. \quad (25)$$

As can be seen, the third-order IFCs of the three studied structures do not show such large differences that could have been expected based on the differences in the calculated RTs. Therefore, it seems that the different RTs are mostly due to the harmonic quantities included in the anharmonic Hamiltonian and some possible reasons for the different RTs of $Na_4[Al_4Si_{19}]$ are discussed next. As mentioned in Sec. II B,

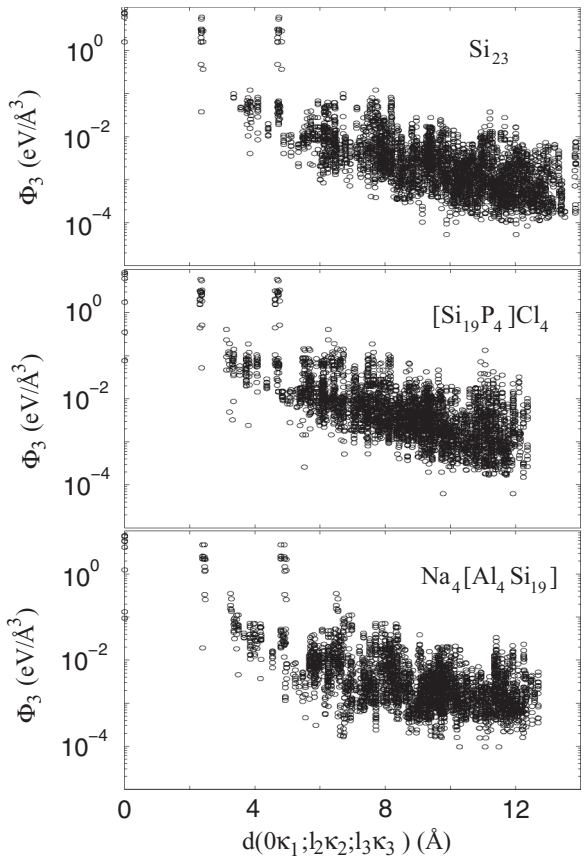


FIG. 6. Calculated third-order IFCs for $Si_{23}$, $[Si_{19}P_4]Cl_4$ and $Na_4[Al_4Si_{19}]$. Here, $d(0\kappa_1;l_2\kappa_2;l_3\kappa_3)$ and $\Phi_3$ are given by Eqs. (24) and (25).

the decrease of mass of the atoms and the term $\omega_\lambda\omega_{\lambda'}\omega_{\lambda'}$ in general decreases the value of the RTs. Also, as $\omega_{\lambda'}$ and $\omega_{\lambda''}$ have smaller values, the following term $(\bar{n}_{\lambda'}+\bar{n}_{\lambda''}+1)$ in Eq. (16) further decreases the value of the RTs (see also Fig. 7). Since the PR values for the acoustic modes in the case of $Na_4[Al_4Si_{19}]$ are rather small (only few atoms vibrate in a particular state), the probabilities $|\mathbf{e}(\kappa|\lambda)|^2$ and thus the phonon eigenvectors $\mathbf{e}(\kappa|\lambda)$ for the acoustic modes are expected to be rather large, which in turn decreases the RTs of these modes through the coefficients $|V(\lambda;\lambda';\lambda'')|^2$. The exponential factors, $e^{i\mathbf{q}_i\cdot\mathbf{x}(l_i)}$, are identical in all structures. Together with the differing $P_3$ and smaller group velocity values of the acoustic modes, these mentioned factors may in part explain the smaller RT and lattice thermal conductivity values of $Na_4[Al_4Si_{19}]$.

The effect of the phase space together with the factors $\omega_\lambda\omega_{\lambda'}\omega_{\lambda'}$ and $(\bar{n}_{\lambda'}+\bar{n}_{\lambda''}+1)$ can be assessed by considering so-called weighted phase space [37] given as $W_3^T(\lambda) = W_3^+(\lambda)+W_3^-(\lambda)$, where [see Eqs. (5) and (16)]

$$W_3^-(\lambda) = \sum_{\lambda'}\sum_{\lambda''}\frac{(\bar{n}_{\lambda'}+\bar{n}_{\lambda''}+1)}{\omega_\lambda\omega_{\lambda'}\omega_{\lambda'}}\delta[\omega_\lambda-\omega_{\lambda'}-\omega_{\lambda''}], \quad (26)$$

and

$$W_3^+(\lambda) = \sum_{\lambda'}\sum_{\lambda''}\frac{(\bar{n}_{\lambda'}-\bar{n}_{\lambda''})}{\omega_\lambda\omega_{\lambda'}\omega_{\lambda'}}\delta[\omega_\lambda+\omega_{\lambda'}-\omega_{\lambda''}]. \quad (27)$$

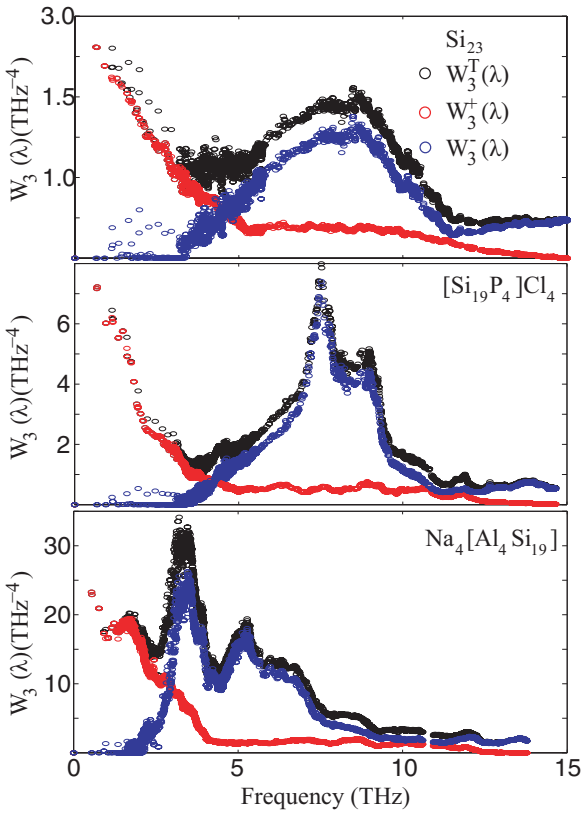


FIG. 7. Calculated weighted phase space for each state λ for $Si_{23}$, $[Si_{19}P_4]Cl_4$, and $Na_4[Al_4Si_{19}]$ at 300 K.

The weighted phase spaces $W_3^T(\lambda), W_3^+(\lambda)$, and $W_3^-(\lambda)$ at 300 K are shown in Fig. 7.

The largest $W_3^T(\lambda)$ values are obtained for the structure $Na_4[Al_4Si_{19}]$ the values being about one order of magnitude larger in comparison to the other two structures. The ratio between $W_3^T(\lambda)$ obtained for different structures is of the same order as the difference in the lattice thermal conductivity at 300 K. The results are in reasonable agreement with the above analysis on the factors $\omega_\lambda\omega_{\lambda'}\omega_{\lambda'}$ and $(\bar{n}_{\lambda'} + \bar{n}_{\lambda''} + 1)$. Moreover, the result obtained for the $W_3^T(\lambda)$ further validates the similarity of the third-order IFCs discussed above. To summarize, the stronger anharmonicity of the structure $Na_4[Al_4Si_{19}]$ in comparison to $Si_{23}$ and $[Si_{19}P_4]Cl_4$ seems to arise mostly from the differing harmonic quantities instead of the third-order IFCs.

One way to measure the anharmonicity of a structure are the so-called Grüneisen parameters. By using the perturbation theory, it has been shown that the Grüneisen parameters can be written as [68]

$$\gamma_{\mu\nu}(\lambda) = -\sum_{j'=4}^{3n} \frac{12V_{\mu\nu}(0j')V(0j';\lambda;-\lambda)}{\hbar^2\omega_{0j'}\omega_\lambda} - \frac{2V_{\mu\nu}(\lambda;-\lambda)}{\hbar\omega_\lambda}, \quad (28)$$

where the first term on the right-hand side vanishes if the position of every atom in the unit cell is determined by the symmetry (no internal strain). In Eq. (28), the coefficients such as $V(\lambda;\lambda';\lambda'')$ are given by Eq. (5) and

$$V_{\mu\nu}(\lambda;\lambda') = \frac{\hbar}{4}\sum_{\kappa,\alpha}\sum_{l',\kappa',\alpha'}\sum_{l'',\kappa''}\Phi_{\alpha\alpha'\mu}(0\kappa;l'\kappa';l''\kappa'') \times \frac{e_\alpha(\kappa|\lambda)e_{\alpha'}(\kappa'|\lambda')}{\sqrt{M_\kappa M_{\kappa'}\omega_\lambda\omega_{\lambda'}}}e^{i\mathbf{q}'\cdot\mathbf{x}(l')}x_\nu(l''\kappa''). \quad (29)$$

The Grüneisen parameters can also be written as

$$\gamma_{\mu\nu}(\lambda) = -\frac{1}{\omega_\lambda}\frac{\partial\omega_\lambda}{\partial\eta_{\mu\nu}}, \quad (30)$$

and furthermore, in the case of cubic crystals

$$\frac{1}{3}\gamma_{\mu\mu}(\lambda) = -\frac{V}{\omega_\lambda}\frac{\partial\omega_\lambda}{\partial V} \equiv \gamma(\lambda). \quad (31)$$

When the phonon-phonon interaction is approximated in the so-called continuum theory, it has been shown that the square of the (averaged) Grüneisen parameter is inversely proportional to the mean-free path and thus the lifetime of phonons [47].

The Grüneisen parameters are sometimes used to calculate the thermal expansion of materials. There is some evidence that, for instance, crystalline materials with negative thermal expansion (NTE) over rather wide temperature ranges can have relatively low lattice thermal conductivity values [69,70] (measured for polycrystalline samples, however). This behavior of NTE materials would be rather logical since, as mentioned, in the continuum theory $\tau \propto \gamma^{-2}$ ($\tau$ and $\gamma$ are some average values) and within so-called quasiharmonic approximation (QHA), the coefficient of thermal expansion (CTE) can be written as (see, for example, Ref. [71]) $\alpha_{\mu_1\nu_1} = \sum_{\mu_2,\nu_2}\sum_\lambda s^T_{\mu_1\nu_1\mu_2\nu_2}c_v(\lambda)\gamma_{\mu_1\nu_1}(\lambda)$, where $s^T_{\mu_1\nu_1\mu_2\nu_2}$ is isothermal second-order compliance tensor, inverse to isothermal second-order elastic constant $c^T_{\mu_1\nu_1\mu_2\nu_2}$. That is, $\{\gamma_{\mu\nu}(\lambda)\}$ are usually expected to have relatively large absolute values for materials that have rather large absolute value of the CTE. There is some evidence that the silicon clathrate framework VII possesses rather unusual NTE behavior, while $Si_{23}$ (or VIII), for instance, has CTE that is rather similar to $d$-Si [72].

The calculated Grüneisen parameter values $\gamma(\lambda)$ as a function of frequency for each structure are shown in Fig. 8. For acoustic modes, the distribution of $\gamma(\lambda)$ values in the case of $Si_{23}$ and $[Si_{19}P_4]Cl_4$ is rather similar, while for $Na_4[Al_4Si_{19}]$ a fairly different result is obtained. Compared with $Na_4[Al_4Si_{19}]$, the maximum values of $\gamma(\lambda)$ are smaller by a factor of about eight in the case of $Si_{23}$ and $[Si_{19}P_4]Cl_4$. For $Na_4[Al_4Si_{19}]$, the lowest-energy optical modes have about three times larger Grüneisen parameter values in comparison to $[Si_{19}P_4]Cl_4$. For $Si_{23}$, the Grüneisen parameter results are similar to those obtained in Refs. [72] and [29].

To study the relationship between the RTs and Grüneisen parameters, these quantities are depicted in Fig. 9 for $Na_4[Al_4Si_{19}]$. For the acoustic modes, when $\gamma(\lambda) \geqslant 2$, the maximum $\tau(\lambda)$ values are approximately $2 \times 10^{-12}$ s, which is about one order of magnitude smaller than the largest values obtained. Thus, these modes have a rather small contribution to the lattice thermal conductivity. The smallest $\tau(\lambda)$ values for the acoustic modes are obtained when the Grüneisen parameters have values between 3 and 4. The relationship shown in Fig. 9 indicates that in some cases, there can be a

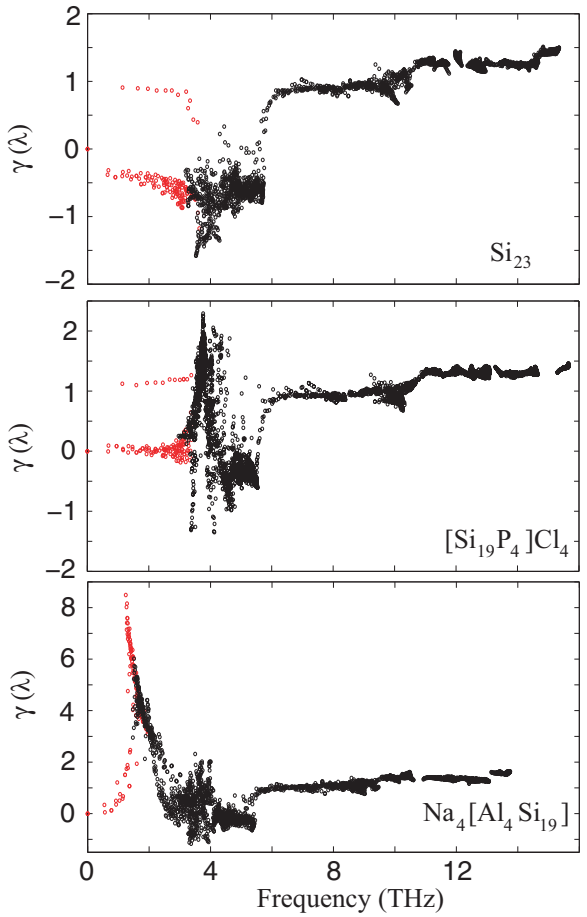


FIG. 8. Calculated Grüneisen parameter values for $Si_{23}$, $[Si_{19}P_4]Cl_4$, and $Na_4[Al_4Si_{19}]$. The acoustic modes are shown in red and the optical modes in black.

connection between the relatively large absolute values of CTE and rather low lattice thermal conductivities.

As already mentioned in Sec. I, several mechanisms have been proposed to explain the rather small lattice thermal conductivity of various Zintl clathrates. In Ref. [17], inelastic neutron scattering data for the $Ba_8Ga_{16}Ge_{30}$ clathrate was used to conclude that the reduction of the lattice thermal conductivity is mostly due to the flattening of the phonon dispersion relations caused by the guest atoms instead of the shorter RTs of the phonons. In Ref. [25], inelastic x-ray scattering and *ab initio* lattice dynamical studies on the $Ba_8Si_{46}$ clathrate resulted in the conclusion that the reduction of the lattice thermal conductivity follows from the changes in the harmonic spectrum induced by the guest-framework interactions and that the reduced RTs have a rather small significance. In contrast, in an *ab initio* lattice dynamical study for the $Ba_8Ga_{16}Ge_{30}$ clathrate [27], the largest reduction in the lattice thermal conductivity was suggested to arise from the smaller RT values, while the reduction of the phonon group velocities was found to have a smaller effect (the BTE was not solved iteratively, but within the single-mode relaxation time approximation).

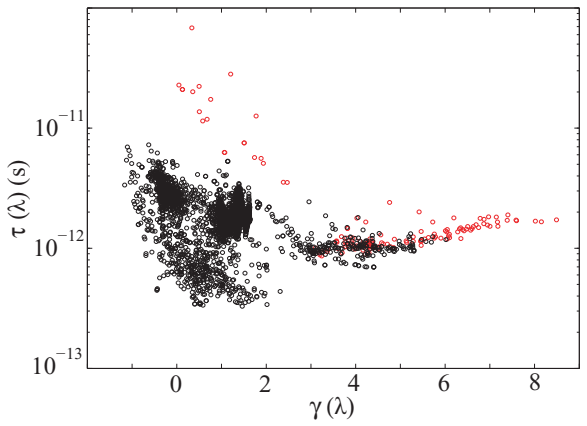


FIG. 9. Calculated RTs versus the corresponding Grüneisen parameter values for each state λ in $Na_4[Al_4Si_{19}]$. The acoustic modes are shown in red and the optical modes in black.

The present results show similarities with the results obtained in Ref. [27] for the $Ba_8Ga_{16}Ge_{30}$ clathrate and in Ref. [38] for the $YbFe_4Sb_{12}$ skutterudite. In particular, the present results are similar to those obtained earlier for the $BaCo_4Sb_{12}$ skutterudite [37]. In the case of $YbFe_4Sb_{12}$ [38], it was summarized that the increased phonon scattering is due to the differing phonon phase space, third-order IFCs having rather marginal effect on the reduction of the lattice thermal conductivity. The results of the present work are in line with the earlier work on the skutterudites [37] and show that for materials with relatively similar third-order IFCs, there can be rather significant changes in anharmonicity and in the lattice thermal conductivity values, which essentially follow from the differing second-order IFCs. To sum up some central findings of the present work: in the case of $Na_4[Al_4Si_{19}]$, the second-order IFCs seem to produce the harmonic phonon spectrum such that three-phonon phase space favors the phonon scattering and the phonon eigenvectors $\mathbf{e}(\kappa|\lambda)$ have rather large values for phonons of smallest frequencies (localization). These effects facilitate the reduction of RTs and phonon group velocities, which in turn leads to the reduced lattice thermal conductivity values. The hypothetical structures studied here possess rather high symmetry (symmetry is forced in the calculation) and it is probable that possible structural disorder decreases the lattice thermal conductivity even further [73,74].

## IV. CONCLUSIONS

The lattice thermal conductivity of the silicon clathrate framework $Si_{23}$ and two Zintl clathrates, $[Si_{19}P_4]Cl_4$ and $Na_4[Al_4Si_{19}]$, was investigated by using *ab initio* lattice dynamics together with an iterative solution of the linearized BTE. The lattice thermal conductivity of the structure $Na_4[Al_4Si_{19}]$ was found to be about one order of magnitude lower at 300 K in comparison to the other two materials studied here. The lower lattice thermal conductivity of $Na_4[Al_4Si_{19}]$ is mostly due to lower relaxation times and phonon group velocities, which differ from $Si_{23}$ and $[Si_{19}P_4]Cl_4$ largely due second-order IFCs. Furthermore, it appears that the anharmonicity of two similar crystalline materials can be rather different from one another mostly because of differing second-order IFCs. Considering the results obtained here

and the earlier results on skutterudites, there is increasing evidence that the preceding may be valid rather generally for various crystal structures. To further reduce the lattice thermal conductivity, one may ask how to modify the harmonic phonon spectrum towards further reductions and at the same time, how to increase the anharmonicity through the third- and higher-order IFCs. The present results may shed light on the understanding about the lattice thermal conductivity of materials such as clathrates and skutterudites, for example, which can give further guidance for the discovery of more efficient thermoelectric materials.

## ACKNOWLEDGMENTS

We gratefully acknowledge funding from the Foundation for Research of Natural Resources in Finland (Grant No. 17591/13). The computing resources for this work were provided by the Finnish Grid Infrastructure (FGI) and CSC - the Finnish IT Center for Science.

[1] A. F. Ioffe, *Semiconductor Thermoelements and Thermoelectric Cooling* (Infosearch Limited, London, 1957), pp. 1–184.
[2] G. A. Slack and D. Rowe, *CRC Handbook of Thermoelectronics* (CRC, Boca Raton, 1995), p. 407.
[3] J. S. Kasper, P. Hagenmuller, M. Pouchard, and C. Cros, Science **150**, 1713 (1965).
[4] G. Nolas, J. Cohn, G. Slack, and S. Schujman, Appl. Phys. Lett. **73**, 178 (1998).
[5] K. A. Kovnir and A. V. Shevelkov, Russ. Chem. Rev. **73**, 923 (2004).
[6] A. J. Karttunen, T. F. Fassler, M. Linnolahti, and T. A. Pakkanen, Inorg. Chem. **50**, 1733 (2010).
[7] T. Takabatake, K. Suekuni, T. Nakayama, and E. Kaneshita, Rev. Mod. Phys. **86**, 669 (2014).
[8] P. Norouzzadeh, C. W. Myles, and D. Vashaee, Sci. Rep. **4**, 7028 (2014).
[9] J. L. Cohn, G. S. Nolas, V. Fessatidis, T. H. Metcalf, and G. A. Slack, Phys. Rev. Lett. **82**, 779 (1999).
[10] J. S. Tse, K. Uehara, R. Rousseau, A. Ker, C. I. Ratcliffe, M. A. White, and G. MacKay, Phys. Rev. Lett. **85**, 114 (2000).
[11] J. Dong, O. F. Sankey, and C. W. Myles, Phys. Rev. Lett. **86**, 2361 (2001).
[12] G. Nolas, M. Beekman, J. Gryko, G. Lamberton Jr, T. Tritt, and P. McMillan, Appl. Phys. Lett. **82**, 910 (2003).
[13] A. Bentien, M. Christensen, J. D. Bryan, A. Sanchez, S. Paschen, F. Steglich, G. D. Stucky, and B. B. Iversen, Phys. Rev. B **69**, 045107 (2004).
[14] M. A. Avila, K. Suekuni, K. Umeo, H. Fukuoka, S. Yamanaka, and T. Takabatake, Phys. Rev. B **74**, 125109 (2006).
[15] K. Suekuni, M. A. Avila, K. Umeo, and T. Takabatake, Phys. Rev. B **75**, 195210 (2007).
[16] Y. Takasu, T. Hasegawa, N. Ogita, M. Udagawa, M. A. Avila, K. Suekuni, and T. Takabatake, Phys. Rev. Lett. **100**, 165503 (2008).
[17] M. Christensen, A. B. Abrahamsen, N. B. Christensen, F. Juranyi, N. H. Andersen, K. Lefmann, J. Andreasson, C. R. Bahl, and B. B. Iversen, Nature Mater. **7**, 811 (2008).
[18] M. Avila, K. Suekuni, K. Umeo, H. Fukuoka, S. Yamanaka, and T. Takabatake, Appl. Phys. Lett. **92**, 041901 (2008).
[19] M. Christensen, S. Johnsen, F. Juranyi, and B. B. Iversen, J. Appl. Phys. **105**, 073508 (2009).
[20] M. Christensen, S. Johnsen, and B. B. Iversen, Dalton Trans. **39**, 978 (2010).
[21] C. Candolfi, U. Aydemir, A. Ormeci, W. Carrillo-Cabrera, U. Burkhardt, M. Baitinger, N. Oeschler, F. Steglich, and Y. Grin, J. Appl. Phys. **110**, 043715 (2011).
[22] H. Euchner, S. Pailhès, L. T. K. Nguyen, W. Assmus, F. Ritter, A. Haghighirad, Y. Grin, S. Paschen, and M. de Boissieu, Phys. Rev. B **86**, 224303 (2012).
[23] J. Fulmer, O. I. Lebedev, V. V. Roddatis, D. C. Kaseman, S. Sen, J.-A. Dolyniuk, K. Lee, A. V. Olenev, and K. Kovnir, J. Am. Chem. Soc. **135**, 12313 (2013).
[24] Y. He and G. Galli, Nano Lett. **14**, 2920 (2014).
[25] S. Pailhès, H. Euchner, V. M. Giordano, R. Debord, A. Assy, S. Gomès, A. Bosak, D. Machon, S. Paschen, and M. de Boissieu, Phys. Rev. Lett. **113**, 025506 (2014).
[26] R. Castillo, W. Schnelle, M. Bobnar, U. Burkhardt, B. Böhme, M. Baitinger, U. Schwarz, and Y. Grin, Z. Anorg. Allg. Chem. **641**, 206 (2015).
[27] T. Tadano, Y. Gohda, and S. Tsuneyuki, Phys. Rev. Lett. **114**, 095501 (2015).
[28] K. Kishimoto, S. Koda, K. Akai, and T. Koyanagi, J. Appl. Phys. **118**, 125103 (2015).
[29] P. Norouzzadeh and C. W. Myles, J. Mater. Sci. **51**, 4538 (2016).
[30] G. K. Madsen, A. Katre, and C. Bera, Phys. Status Solidi A **213**, 802 (2016).
[31] B. Chen, J.-H. Xu, C. Uher, D. T. Morelli, G. P. Meisner, J.-P. Fleurial, T. Caillat, and A. Borshchevsky, Phys. Rev. B **55**, 1476 (1997).
[32] G. S. Nolas, J. L. Cohn, and G. A. Slack, Phys. Rev. B **58**, 164 (1998).
[33] G. Nolas, D. Morelli, and T. M. Tritt, Annu. Rev. Mater. Sci. **29**, 89 (1999).
[34] B. C. Sales, B. C. Chakoumakos, and D. Mandrus, Phys. Rev. B **61**, 2475 (2000).
[35] M. Puyet, B. Lenoir, A. Dauscher, M. Dehmas, C. Stiewe, and E. Müller, J. Appl. Phys. **95**, 4852 (2004).
[36] X. Shi, H. Kong, C.-P. Li, C. Uher, J. Yang, J. R. Salvador, H. Wang, L. Chen, and W. Zhang, Appl. Phys. Lett. **92**, 182101 (2008).
[37] W. Li and N. Mingo, Phys. Rev. B **89**, 184304 (2014).
[38] W. Li and N. Mingo, Phys. Rev. B **91**, 144304 (2015).
[39] V. Baran, A. Senyshyn, A. J. Karttunen, A. Fischer, W. Scherer, G. Raudaschl-Sieber, and T. F. Fässler, Chem. Eur. J. **20**, 15077 (2014).
[40] Y. Dong, P. Chai, M. Beekman, X. Zeng, T. M. Tritt, and G. S. Nolas, Inorg. Chem. **54**, 5316 (2015).
[41] F. Sui, H. He, S. Bobev, J. Zhao, F. E. Osterloh, and S. M. Kauzlarich, Chem. Mater. **27**, 2812 (2015).
[42] K. Huang and M. Born, *Dynamical Theory of Crystal Lattices* (Clarendon Press, Oxford, 1954), pp. 293–306.

[43] A. Maradudin, E. Montroll, G. Weiss, and I. Ipatova, *Theory of The Lattice Dynamics in The Harmonic Approximation*, Vol. Supplement 3 (Academic Press, New York, 1971), pp. 6–57.
[44] A. Maradudin and G. Horton, *Elements of The Theory of Lattice Dynamics*, Vol. 1 (North-Holland, Amsterdam, 1974), pp. 1–82.
[45] V. J. Härkönen and A. J. Karttunen, Phys. Rev. B **93**, 024307 (2016).
[46] V. J. Härkönen, arXiv:1603.06376 (unpublished).
[47] J. M. Ziman, *Electrons and Phonons: The Theory of Transport Phenomena in Solids* (Oxford University Press, Oxford, 1960), pp. 264–298.
[48] G. P. Srivastava, *The Physics of Phonons* (CRC Press, Boca Raton, 1990), p. 122.
[49] M. Omini and A. Sparavigna, Physica B **212**, 101 (1995).
[50] M. Omini and A. Sparavigna, Phys. Rev. B **53**, 9064 (1996).
[51] A. Ward, D. A. Broido, D. A. Stewart, and G. Deinzer, Phys. Rev. B **80**, 125203 (2009).
[52] W. Li, J. Carrete, N. A. Katcho, and N. Mingo, Comput. Phys. Commun. **185**, 1747 (2014).
[53] A. Maradudin and A. Fein, Phys. Rev. **128**, 2589 (1962).
[54] L. Paulatto, I. Errea, M. Calandra, and F. Mauri, Phys. Rev. B **91**, 054304 (2015).
[55] A. H. Romero, E. K. U. Gross, M. J. Verstraete, and O. Hellman, Phys. Rev. B **91**, 214310 (2015).
[56] K. Momma and F. Izumi, J. Appl. Crystallogr. **44**, 1272 (2011).
[57] A. Shevelkov and K. Kovnir, Struct. Bond. **139**, 97 (2011).
[58] C. Gatti, L. Bertini, N. P. Blake, and B. B. Iversen, Chem. Eur. J. **9**, 4556 (2003).
[59] P. Giannozzi, S. Baroni, N. Bonini, M. Calandra, R. Car, C. Cavazzoni, D. Ceresoli, G. L. Chiarotti, M. Cococcioni, I. Dabo, A. Dal Corso, S. de Gironcoli, S. Fabris, G. Fratesi, R. Gebauer, U. Gerstmann, C. Gougoussis, A. Kokalj, M. Lazzeri, L. Martin-Samos, N. Marzari, F. Mauri, R. Mazzarello, S. Paolini, A. Pasquarello, L. Paulatto, C. Sbraccia, S. Scandolo, G. Sclauzero, A. P. Seitsonen, A. Smogunov, P. Umari, and R. M. Wentzcovitch, J. Phys.: Condens. Matter **21**, 395502 (2009).
[60] K. F. Garrity, J. W. Bennett, K. M. Rabe, and D. Vanderbilt, Comput. Mater. Sci. **81**, 446 (2014).
[61] J. P. Perdew, K. Burke, and M. Ernzerhof, Phys. Rev. Lett. **77**, 3865 (1996).
[62] W. Li, N. Mingo, L. Lindsay, D. A. Broido, D. A. Stewart, and N. A. Katcho, Phys. Rev. B **85**, 195436 (2012).
[63] W. Li, L. Lindsay, D. A. Broido, D. A. Stewart, and N. Mingo, Phys. Rev. B **86**, 174307 (2012).
[64] R. J. Bell, P. Dean, and D. C. Hibbins-Butler, J. Phys. C **3**, 2111 (1970).
[65] J. Hafner and M. Krajci, J. Phys.: Condens. Matter **5**, 2489 (1993).
[66] C. D. Meyer, *Matrix Analysis and Applied Linear Algebra* (SIAM, Philadelphia, 2000).
[67] L. Lindsay and D. Broido, J. Phys.: Condens. Matter **20**, 165209 (2008).
[68] T. Barron, M. Klein, G. Horton, and A. Maradudin, *Perturbation Theory of Anharmonic Crystals*, Vol. 1 (North-Holland, Amsterdam, 1974), pp. 391–450.
[69] C. A. Kennedy and M. A. White, Solid State Commun. **134**, 271 (2005).
[70] C. A. Kennedy, M. A. White, A. P. Wilkinson, and T. Varga, Appl. Phys. Lett. **90**, 151906 (2007).
[71] D. Wallace, *Thermodynamics of Crystals* (Wiley, New York, 1972).
[72] V. J. Härkönen and A. J. Karttunen, Phys. Rev. B **89**, 024305 (2014).
[73] B. Chakoumakos, B. Sales, D. Mandrus, and G. Nolas, J. Alloys Compd. **296**, 80 (2000).
[74] B. Chakoumakos, B. Sales, and D. Mandrus, J. Alloys Compd. **322**, 127 (2001).